Received: 14 August 2025

Accepted: 23 October 2025

Published: 06 November 2025

# Real Time Operation of Microgrid with Variation of Distribution Generation Source to IEEE 13 Bus System

Sunil Kumar 1\*, Ikbal Ali 2, and Anwar Shahzad Siddiqui 3

<sup>1</sup>\*2.3 Jamia Millia Islamia, Department of Electrical Engineering, New Delhi, India

\*skk7503@gmail.com, iali1@jmi.ac.in, assiddiqui@jmi.ac.in

#### **Abstract**

As the world energy sector shifts to renewable energy sources (RES), microgrids (MGs) are becoming more important for providing reliable and efficient power. MGs can effectively integrate distributed renewable generation in the grid connected and islanded modes and ensure system reliability. This paper presents a new type of Master-Slave (MS) allocation algorithm for distributed generation (DG) planning in microgrids. Unlike the conventional methods in which all DG units operate at unity power factor (UPF), the MS is implemented with one DG as a master (operating at nonunity power factor) and two DGs as slaves (operating at UPF). This setup optimizes the allocation of DG and minimizes power losses under variable loading conditions. The proposed MS-based model is integrated with the Particle Swarm Optimization (PSO)-Fast Decoupled Load Flow (FDLF) algorithm in order to find optimal placement of master and slave DGs. Simulation on the IEEE-13 bus test system reveals that the proposed scheme decreases real power losses up to 77% compared to the base case without DG and 45% compared to PSO-NR optimization. In addition, the minimum bus voltage is increased from 0.90 p.u. (without DG) to 0.973 p.u. (with PSO-FDLF), thus satisfying the voltage stability constraints in all load scenarios. Validation in the RTDS/RSCAD platform shows that the optimized MS configuration is able to guarantee voltage deviation within  $\pm$  3% of nominal values with significant reduction of active power losses as well as reactive power losses. These results show that the proposed MS-based optimization framework offers a robust and scalable solution for the improvement of microgrid performance, which is of direct interest for utility operators operating in renewable embedded environments.

**Index-words:** Distributed Generation, Microgrid, Renewable Energy Source, Real time digital simulator, Variable Loads.

Nomenclature			
BPSO	Binary Particle Swarm Optimization		
DG	Distributed Generation		
DERs	Distributed Energy Sources		
DEO	Dolphin Echolocation Optimization		
$E_f$	Variable Field Voltage		
FDLF	Fast Decoupled Load Flow		
$F_{ob}$	Objective Function		
$l_d$	Demand Level		
MG	Microgrid		
MS	Master-Slave		
MPPT	Maximum Power Point Tracking		
PSO	Particle Swarm Optimization		
$P_{loss,mn}^d$	Power Loss between bus m and n		
$P_{Gm}$	Active Power Generation at bus m		
$P_{Dm}$	Active Power Demand at bus m		

PV	Photovoltaic
$P_m$	Mechanical Power
$P_e$	Electrical Power
$Q_{Gm}$	Reactive Power Generation at bus m
$Q_{Dm}$	Reactive Power Demand at bus m
RSCAD	Real Time Digital Simulator Computer Aided Design
RTDS	Real Time Digital Simulator
RES	Renewable Energy Source
SMA	Slime Mould Algorithm
$t_{DGs}$	Aggregate Number of DGs
UPF	Unity Power Factor
WOA	Whale Optimization Algorithm
WT	Wind Turbine
$x_m, y_m$	Voltage Constraint
NR	Newton Raphson



#### I. Introduction

#### A. Motivation

The introduction of distributed generation to the grid boosts interest in microgrids. The independence of operation of microgrids is a part of the major anticipated characteristics of modern smart grids. A common configuration of a microgrid includes solar panels, wind turbines (WT), and a diesel generator [1]. The study found in [2], [3] investigated different approaches to selecting the right location and power size for DGs to operate distribution systems in the most effective way. The ability of microgrids to operate autonomously and integrate with the larger grid allows for increased flexibility and adaptability in energy management. As the world transitions towards a more decentralized and sustainable energy future, the examination and optimization of microgrid technologies become increasingly relevant for achieving a robust and environmentally sustainable power infrastructure [4]. The intermittent nature of renewable resources such as sunlight and wind makes real-time operation of microgrids essential in ensuring the stability and effectiveness of the process. As mentioned in previous research [5], [6], [7], to enhance the flexibility and adaptability of energy management, microgrid-based system designs are beneficial. However, the intermittent characteristics of renewable sources tend to create uncertainty in the power production in microgrids, highlighting the necessity of powerful operational methodologies and optimization models capable of guaranteeing a stable and reliable operation of the real-world scenario.

#### B. Research gap

Despite the progress on the development of microgrid technologies and their connection to modern power grids, there is a gap in the literature related to the real-time operational problems of microgrids under variable DG conditions. Previous research has been largely focused on steady-state control methods or economic optimization, since these approaches fail to address the variability of RES. In this research work, the IEEE-13 bus system is used as a common benchmark test case for validating the proposed methodology, but the identified research gap is a general application for microgrids regardless of the selected test system. Existing literature suggests that the optimal placement of distributed generators can provide either technical or economic

benefits, but methods for microgrid control [8] or the influence of component placement on system stability [9] do not offer a comprehensive approach to operating microgrids, as energy from solar and wind power sources fluctuates in real-time. Economic objectives, such as profit maximization and operational cost minimization, are commonly considered in DG allocation studies [10]. Most existing research on autonomous microgrid operation is now focusing on its operational aspects. Previous research [11], [12] focused on enhancing stability, developing control methods for maintaining stable operation, and improving power quality by reducing harmonic distortion [13], [14]. According to the planning approach [15], the most suitable type of DG is selected for a grid-connected microgrid, which considers fixedsize DGs operated with UPF to minimize the losses and investment cost of distributed energy sources. Genetic algorithm [16] is used to optimize DGs placement and sizing to reduce power loss and improve voltage profile; however, it did not focus on real-time control. A two-stage robust optimization approach [17] accommodates the uncertainties in the energy generated by the DG and the energy needed by the grid. Since Mixed-Integer Programming can be very complex, the solution might take too much time for real-time situations. A proposed energy management [18] operational strategy was proposed that entails the most appropriate combination and diversity of DERs. However, this study did not account for the optimization of the distributed generation locations. A cost-effective method is employed by installing an optimal size DG at strategic locations with an estimated reliability standard [19]. This approach failed to tackle the practical difficulties associated with integrating such solutions into current distribution systems. In the existing study [20], the researcher exclusively focused on variations in real power generation and demand. A comprehensive study in [21] explored the optimization of reactive power planning within microgrids. The performance of microgrids is determined by looking at voltage limit constraints, especially at times when distributed generators are operating at UPF. To improve solar PV source power forecasting and minimize uncertainty, a hybrid EMD-PSO-ANFIS model is suggested to handle the variability of renewable DG sources. Likewise, ANFIS-based strategies have been implemented to guarantee the reliability of PV systems, considering the sustainability of the performance and wellbeing of DG assets embedded in microgrids [22], [23]. The work in [24] emphasizes the importance and

excellence of the Computational Intelligence (CI) technologies, including PSO, to renewable energy systems. It gives the selected methodology a good basis and connects the specific application to a bigger and long-established trend of using CI in power systems.

An approach in [25] determines the optimal location of DGs within a standalone microgrid to meet realtime active power demands, supported by distributed reactive power sources for injecting reactive power. Droop control [26] and the Master-slave technique with Particle Swarm Optimization-Newton Raphson (PSO-NR) [27] are applied to handle DG insertion and placement in isolated microgrids. In droopbased control, the system frequency and voltage are adjusted using only the actual and reactive power, and this action can change the system's voltage and frequency levels. A small microgrid was optimized using genetic algorithms [28], and the efficiency depended on both the number of iterations and how the objective function scores were configured. However, the study does not focus on issues such as the loss of battery capacity, natural battery drains, and the cost of storage space. The method presented in [29] leads to less energy loss from DGs when compared with traditional solutions. The report fails to address the economic implications of variations in renewable energy supply. The previous study suggested different approaches as described in [30] for the design of a stochastic DG allocation scheme. However, the study did not address operational issues and provided little insight into how the model could be implemented in the field. Advanced control strategies [31] improve the efficiency and reliability of DC microgrids by integrating DG. Integrating multiple DG technologies is recognized as a challenging process, with a viable solution currently accessible only to a limited degree. For DG allocation, Particle Swarm Optimization (PSO), Whale Optimization Algorithm (WOA), Dolphin Echolocation Optimization (DEO), and Slime Mould Algorithm (SMA) [32] were tested, and SMA yielded the greatest decrease in losses and a better voltage profile. Still, inadequately sized or placed DG units can cause negative consequences and expensive installations. The Adaptive Bayesian Sparse Polynomial Chaos Expansion (APSPCE) technique presented in [33] is used to address the voltage balance in an isolated microgrid under challenging peak load conditions.

The load generation model [34] states that

deterministic planning poses a significant challenge when considering wind-powered, intermittent, and distributed generators as well as stochastic loads. The controlled method [35] has been proposed to improve the allocation and selection of renewable energy types within a designated distribution network. Despite the abundance of existing research, none of the previous studies considered the most effective operational method (Master versus Slave) of distributed generators when determining the optimal placement of distributed generation in microgrids. The components of a microgrid and their associated challenges are relatively straightforward to understand and categorize. However, the integration of these components creates a realtime microgrid system, making the study more challenging [36].

#### C. Contribution

Unlike conventional distributed generation planning methods in which all units operate at UPF, this study proposes a Master-Slave allocation strategy where one DG operates at a non-unity power factor while the remaining units function as slaves at UPF. This configuration, when integrated with the PSO-FDLF algorithm, enables optimal DG placement to minimize power losses and enhance voltage stability under varying load conditions. The performance of the proposed model is tested through real-time simulations on RTDS using the RSCAD platform, ensuring its practical applicability for microgrid operation. While prior study [37] focused on mathematical models and interactivelevel simulations, no existing work has combined microgrid optimization with real-time simulation frameworks of this kind. In the first phase, the PSO-FDLF algorithm identifies the optimal DG locations within the IEEE 13-bus distribution system, reducing system losses and improving voltage profiles. In the second phase, RTDS/RSCAD simulations provide real-time validation of the proposed method, offering accurate dynamic assessments under diverse loading conditions. The final contribution of this work is the establishment of a Master-Slave allocation framework for DGs utilizing diesel, solar, and wind energy sources. By employing this strategy, the microgrid demonstrates improved operational reliability, reduced losses, and stable voltage regulation across a wide range of load scenarios. The proposed approach thus offers a robust and scalable solution for enhancing microgrid performance in renewable-integrated environments.

This research manuscript is described in five sections. Section 1 is the introduction section. The concepts of the proposed approach and modelling of microgrids are discussed in detail in Sections 2 and 3. The proposed approach is illustrated with its simulation and results in Section 4. Section 5 summarizes the study's overall conclusions.

### II. Purposed approach

The main purpose of the proposed technique is to find out the optimal location of DGs to improve the voltage profile and reduce energy losses in autonomous microgrids. The optimization algorithm is designed to strategically position DGs within the microgrid and determine their operating mode (whether master or slave mode), with the objective of achieving minimal energy losses. Therefore, the objective function of the optimization problem [38] is,

$$F_{ob} = \min \sum_{n=1}^{N} \sum_{m=1}^{N} \sum_{d=1}^{D} P_{loss,mn}^{d}$$
 (1)

In this context, d represents the index of the specific state (d  $\in$  D), while the power loss obtained between the sending and receiving ends of the transmission line that links bus m to bus n is represented by  $P_{loss,mn}^d$ , specifically in the  $d^{th}$  state.

## A. Constraints for active and reactive power balance

Standard load flow analysis, as described in [39], is utilized under stable operating conditions, and it is depicted as follows:

$$P_{Gm}^{d} - \frac{P_{Dm}*l_d}{P_{Dm}^{d}} = \sum_{n=1}^{N} V_m^d V_n^d Y_{mn} \cos(\theta_{mn} + \delta_n^d - \delta_m^d)$$
 (2)

$$Q_{Gm}^{d} - \frac{Q_{Dm}^{*l_d}}{Q_{Dm}^{d}} = -\sum_{n=1}^{N} V_m^d V_n^d Y_{mn} \sin(\theta_{mn} + \delta_n^d - \delta_m^d)$$
 (3)

The voltage at bus m is represented by its magnitude, denoted as  $V_m^d$ , and its phase angle, denoted as  $\delta_m^d$ . For bus m and bus n linking the branch of the bus admittance matrix, the angle is denoted by  $\theta_{mn}$ , and the magnitude is represented by  $Y_{mn}$ .  $P_{Gm}^d$  and  $P_{Dm}$  signify the active power generation and the active power demand, respectively, at bus m for a given state. For the specified state, the reactive power generated at bus m and the reactive power required at bus m are denoted as  $Q_{Gm}^d$  and  $Q_{Dm}$ , respectively. In Table 1, the p.u. Values of demand level  $(l_d)$  are related to the peak consumption. Furthermore, the system must be designed by observing the

restrictions set by the flow of the lines, as explained below:

$$\sqrt{\left(P_{m,n}^d\right)^2 + \left(Q_{m,n}^d\right)^2} \le S_{m,n}^{max} \tag{4}$$

Where  $P_{m,n}^d$  stands for active power and  $Q_{m,n}^d$  stands for reactive power, which is the flow between bus m and bus n, while the thermal limit of the transmission line capacity is denoted by  $S_{m,n}$  and measured in megavolt-amperes (MVA).

Table 1: Demand states

Demand state (d)	Demand level ( $l_d$ ) MW
1	1.70
2	2.40
3	3.47

#### B. Constraints for DG mode selection

 $x_m$  and  $y_m$  are two binary variables, used to ascertain the operational mode of the DG unit, determining whether it operates as a Master or Slave, as well as its placement. The configuration of these variables determines the role of DGs, whether they operate as a master or Slave, is linked to bus m, and set in the corresponding mode. When DG unit is installation at a bus, the variable  $y_m$  is automatically assigned a value of 1. If the DG unit is designated as a Master,  $x_m$  is set to 1; otherwise, if it functions as a Slave,  $x_m$  is set to the initial value 0. The constraint allowed in the system for determining the total number of Master DGs and salve DGs is as follows:

$$\sum_{m=1}^{N} x_m = k \tag{5}$$

$$\sum_{m=1}^{N} y_m = t_{DGs} \tag{6}$$

The number of Master distributed generators in the system is denoted by k. The system maintains a constant value of k, which is always 1, when configured to support only a single master unit. Thus,  $t_{DGs}$  represent the aggregate number of DGs installations necessary to fulfill the demand of the selected modified system. In the modified system,  $y_m = t_{DGs}$  signifies the total number of DGs employed for determining the overall number of DGs. For each Master DG at a bus,  $y_m$  is set to 1 (when  $x_m = 1$ ), a required additional constraint is implemented as follows:

$$y_m \ge x_m \tag{7}$$

#### C. Constraints for Master-Slave generation

The master-slave DG unit has the capability to operate in either a master or a slave mode. When a master DG is set at master mode, it supplies the active and reactive power required by the load. Slave DGs only operate at UPFs, and they supply active power. The permissible time intervals for generating both active and reactive power differ based on the DG's master-slave mode, as illustrated by the following information:

$$P_{primary}^{min} \le P_{Gprimary} \le P_{primary}^{max}$$
 (8)

$$Q_{primary}^{min} \le Q_{Gprimary} \le Q_{primary}^{max}$$
 (9)

$$P_{Gsecondary} = S_{fixed} (10)$$

$$Q_{Gsecondary} = 0 p.u. (11)$$

 $P_{primary}^{min}$  and  $P_{primary}^{max}$  represent the lowest and highest permissible limits for the active power output ( $P_{Gprimary}$ ) of the Master distributed generator. In parallel,  $Q_{primary}^{min}$  and  $Q_{primary}^{max}$  represent the permissible minimum and maximum limits of the reactive power output ( $Q_{Gprimary}$ ) of the master DG unit. Conversely, the Slave DG consistently supplies an active power output of  $P_{Gsecondary}$  and zero reactive power ( $Q_{Gsecondary}$ ).  $P_{Gprimary}$  and  $Q_{Gprimary}$  are continuous variables, whereas  $P_{Gsecondary}$  is a fixed parameter set at a constant value  $S_{fixed}$ .

The constraints described in Eqs. (8) = (10) have been restructured to provide new constraints in the scope of power restriction limitations, which can be expressed as follows:

$$P_{Gm} \le x_m P_{primary}^{max} + (1 - x_m) P_{Gsecondary} Y_m$$
 (12)

$$P_{Gm} \ge x_m P_{primary}^{min} + (1 - x_m) P_{Gsecondary} Y_m$$
 (13)

$$Q_{Gm} \le x_m Q_{primary}^{max} + (1 - x_m) Q_{Gsecondary} Y_m$$
 (14)

$$Q_{Gm} \ge x_m Q_{primary}^{min} + (1 - x_m) Q_{Gsecondary} Y_m$$
 (15)

Here,  $Q_{secondary}$  is assigned a value of 0 p.u. to simulate the operation of the Slave DG at UPF. The

constraints in Eqs. (12) – (15) illustrate the relation between the permissible lower and upper limits of active and reactive power in relation to the location and operational mode of each DG.

#### D. Constraint for MG voltage

The modified IEEE-13 bus system imposes voltage regulation constraints, requiring the voltage levels at the buses to remain within a span of  $\pm$  5%. Thus, the maximum and minimum permissible voltage limits are defined as 1.05 p.u. and 0.95 p.u. Respectively. The voltage at the connected node is maintained at 1.0 p.u. However, slave DG acts as a controlled current sources, which provide a constant active power. Therefore, the voltage limit constraints for any bus, whether connected to a Slave DG or not, are as follows:

$$V_{min} \le V_m^d \le V_{max} \tag{16}$$

$$V_m^d \ge x_m \tag{17}$$

$$V_m^d \le 2 - x_m \tag{18}$$

To elaborate on this, consider a scenario where a Master DG has been assigned to bus 1 ( $x_1 = 1$ ), according to Eqs. (17) and (18), the voltage limits become  $V_1 \geq 1$  and  $V_1 \leq 1$ ; bus one voltage is set to 1 p.u. by default. If bus one is linked to a Slave-controlled DG, then  $x_1 = 0$ . Substituting this into Eqs. (17) and (18), the voltage limit becomes  $0 \leq V_1 \leq 2$ . The limitations of Eq. (16) also apply to bus 1, which makes the voltage not exceed the stated limits of 0.95 and 1.05 p.u.

#### E. PSO-FDLF optimization

The proposed methodology, PSO, is used in the MG system to address the location and optimal position of the master and slave DG units. The FDLF algorithm is used to estimate the load flow, voltage profile, and power losses of each candidate solution generated by PSO. To determine the optimal arrangement of the Master and Slave DGs in the IEEE 13-bus system, a PSO-FDLF based optimization model is suggested and the objective is expressed in Eq. (1). The proposed algorithm achieves near-optimal results by utilizing the principles of swarm intelligence from PSO, which is influenced by both the individual best results of each particle and the global best results of the swarm, as first described in [40]. The optimization

process begins with a random arrangement of the DG locations, which are represented by particles' positions. The Fast Decoupled Load Flow method is employed in each iteration to determine system losses and evaluate particle fitness. The velocity of each particle is adjusted in accordance with three Master considerations: previous velocity  $(v_p^{iter})$ , best known position  $(x_{k,best}^{iter})$ , and the global best position  $(x_{g,best}^{iter})$  found so far. These are adjusted by using two random coefficients  $(rand_1 \text{ and } rand_2)$  and three weighting parameters  $c_1$ ,  $c_2$  and  $c_3$ , where the parameter  $c_1$ ,  $c_2$  are set to 2 and parameter  $c_3$  is gradually decreases from 0.9 to 0.4 during iterations to balance the algorithm's ability to search and pick the best option. The position vector  $(c_3)$  is described by the given equation:

$$x_p^{iter+1} = x_p^{iter} + v_p^{iter+1} \tag{19}$$

$$\begin{aligned} x_p^{iter+1} &= w * v_p^{iter} + c_1 * rand_1 \left( x_{k,best}^{iter} - x_p^{iter} \right) \\ &+ c_2 * rand_2 \left( x_{g,best}^{iter} - x_p^{iter} \right) \end{aligned} \tag{20}$$

The velocity vector of each particle throughout the optimization is updated with the help of Eqs. (20).

The Binary Particle Swarm Optimization (BPSO) approach, using a sigmoid function, is applied to judge the best way to allocate slave DGs  $(y_m)$ . The sigmoid function is used to map the continuous velocity into a quick decision, ensuring the correct handling of placement variables. The sigmoid function is defined as,

$$v_p^{iter+1} = sigm(v_p^{iter+1}) = \frac{1}{1+e^{-v_p^{iter}}}$$
 (21)

The calculation of the particle's new position is done with this probabilistic rule based on the updated velocity:

$$x_p^{iter+1} = \begin{cases} 1 & if \ rand_3 \leq sigm(v_p^{iter+1}) \\ 0 & otherwise \end{cases}$$
 (22)

where  $rand_3$  is a number chosen randomly from the range [0,1].

For this problem, BPSO initializes a binary matrix to decide on a slave bus location, which is denoted by

 $y_m$ . The fitness function is defined as,

$$fitness = \frac{1}{\sum_{n=1}^{N} \sum_{m=1}^{N} \sum_{m=d}^{D} P_{loss,mn}^{d} * t_d}$$
 (23)

Where  $t_d$  is denoted as the time of the multi-period demand state (d). In the proposed optimization, the interaction between PSO and FDLF is considered as the core of the optimization. PSO investigates possible DG allocations, updating particle positions, and FDLF is implemented after every iteration to quickly calculate bus voltages, line flows, and power losses. Such a mixed interaction is vital so that the search in the swarm is always informed based on realistic power flow results, and not mere heuristic guesses. In contrast to traditional NR-based load flow, FDLF has less computational complexity and evaluates more quickly, allowing the nearly real-time optimization of DG location in changing load conditions. The PSO algorithm, which makes use of the FDLF approach, is explained in detail in Algorithm 1.

#### Algorithm 1: PSO with Fast Decoupled Load Flow

Initialize a particle vector with integer constants For each bus having a single Master unit, **do** 

while iterations ≠ maxiterations do

for each particle do

Update the bus data using initial conditions Perform Fast Decoupled Load Flow to calculate the losses

Calculate the fitness

if fitness > best value then

Update the value and new kbest

end if

#### end for

Choose the particle with the best fitness value of all particles as gbest

Calculate the Sigmoid function

Update the new velocity and particle velocity vector

end while

#### end for

Select the maximum fitness for all buses Calculate losses using Fast Decoupled Load Flow

The flowchart of the overall proposed methodology is depicted in Fig. 1.

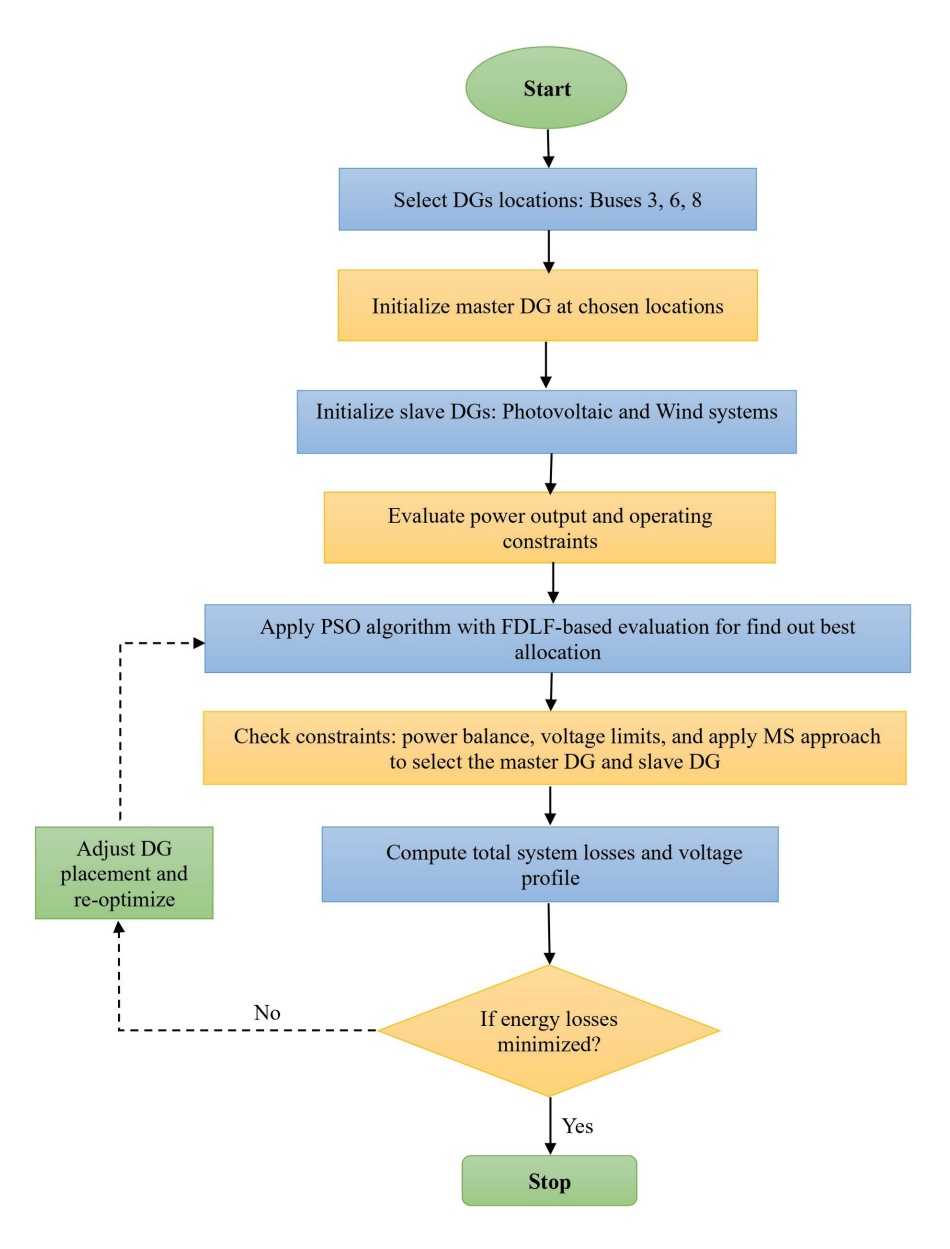


Figure 1: Flowchart of proposed approach.

Such an iterative process also enables PSO to direct the search to solutions with minimum energy losses and stable voltages, and FDLF gives the correct system-level validation of each solution. The approach to PSO and FDLF makes the methodology ideal not only in ensuring an optimal allocation of DG but also in providing accurate judgments of microgrid performance under different conditions of load.

### III. Modelling of microgrid

A modified IEEE 13-bus system, as depicted in Fig. 2, is designed to investigate the impact of the MS method on system losses. The microgrid is heavily loaded with a rated voltage of 4.1 kV for the 13-bus

feeder. The power losses occurring in the system are significantly affected by the kind of distributed generation linked to a bus, whether it functions as a Master or Slave. To assess the importance of the type of connection for distributed generation, three arbitrary candidate locations at buses 3, 6, and 8 were selected in the test system. A single Master DG unit with a maximum threshold of 0.6 p.u. for active power and 0.354 p.u. for reactive power is featured at this location. Furthermore, two Slave distributed power generation systems are in operation, with photovoltaic (PV) systems supplying 0.348 p.u. of constant active power and wind systems supplying 0.16 p.u. of constant active power, both operated at a UPF.

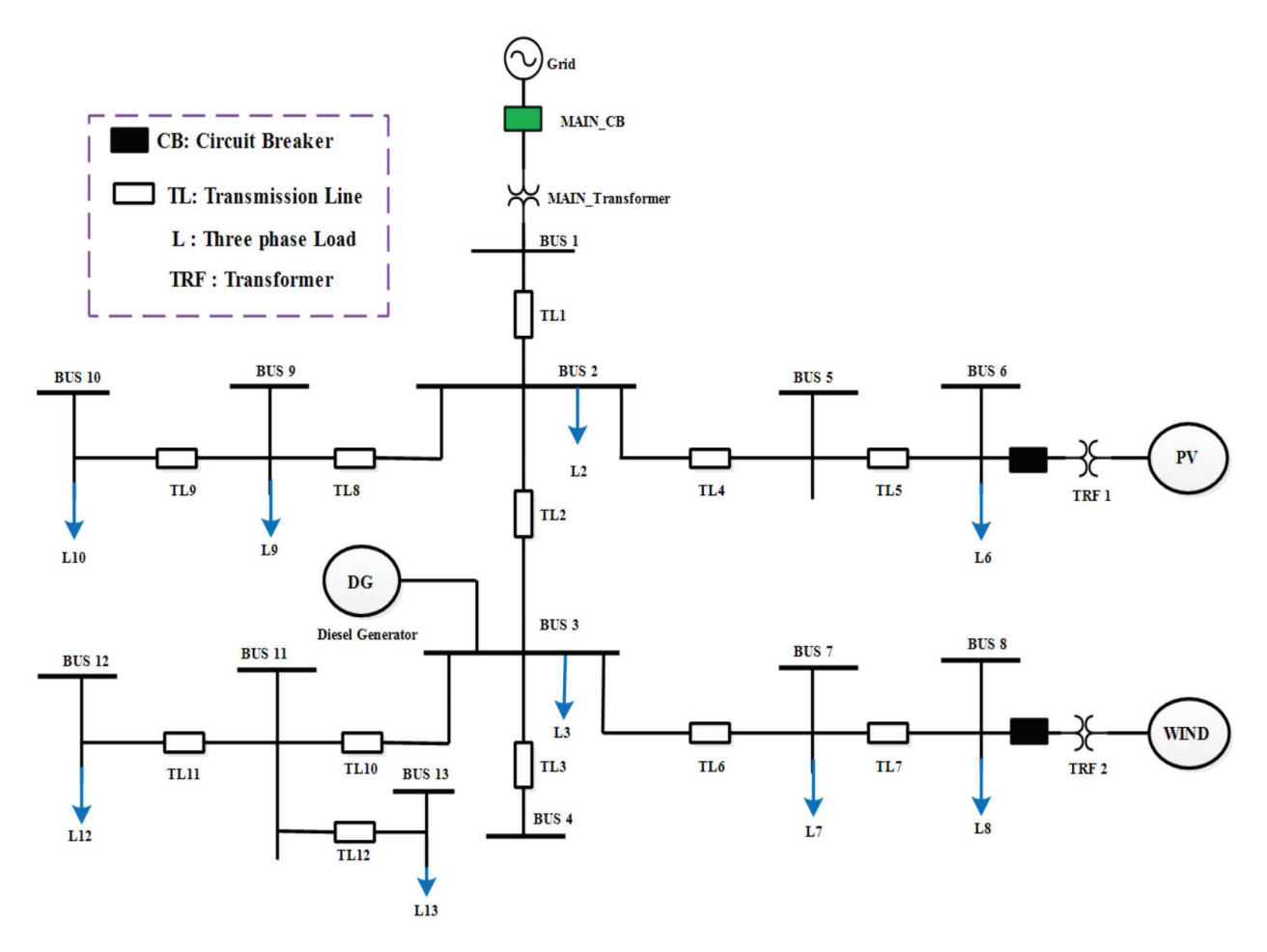


Figure 2: IEEE-13 bus test system under consideration.

The overall power losses are meticulously determined as the Master distributed generation location is systematically varied across the three possible buses. A detailed examination of the operational mode of DGs is crucial, as shown in Table 2. This illustrates how relocating the master DG across the three possible buses affects the system's power losses. However, the optimal configuration is attained when the Master distributed generation is coupled with bus 3, while the Slave distributed generation is interconnected with buses 6 and 8. This configuration results in the lowest power loss, measured at 0.0012 per unit (p.u.).

Table 2: Losses of power in different MS arrangements

Master DG	Slave DG	Power losses based on p.u.
3	8 & 8	0.0012
8	3&6	0.0296
6	3&8	0.1780
3	8 & 8	0.0012

## A. Transmission line and load modifications

The IEEE-13 bus test feeder represents a heavily loaded system, featuring three-phase loads with

variable real power and reactive power connected in a Y-configuration. In Simulation modeling, the dynamic response of the three-phase balanced loads is simulated through a three-phase dynamic load block. The specific details about the transmission line parameters and the connected load are illustrated in Tables 3 and 4, respectively.

Table 3: Transmission line parameters

Line buses		Line Impedance		
From	То	R, p.u.	X, p.u.	
1	2	0.0379	0.01114	
2	3	0.0379	0.01114	
3	4	0.019	0.0557	
2	5	0.0206	0.0323	
5	6	0.11	0.2	
2	9	0.0364	0.0369	
9	10	0.0218	0.0221	
3	7	0.0218	0.0122	
7	8	0.0218	0.0122	
3	11	0.0217	0.0223	
11	12	0.0218	0.0221	
11	13	0.0588	0.0224	

Table 4: Three-phase load scenario

Load on bus	Load Scenario 1		Load Scenario 2		Load Scenario 3	
	$P_D$ p.u.	$Q_{\scriptscriptstyle D}$ p.u.	$P_D$ p.u.	$Q_{\scriptscriptstyle D}$ p.u.	$P_{D}$ p.u.	$Q_D$ p.u.
2	0.024	0.0042	0.03	0.004	0.04	0.0232
3	0.0024	0.0022	0.16	0.028	0.231	0.132
6	0.184	0.0024	0.04	0.008	0.08	0.058
7	0.0158	0.0046	0.028	0.004	0.034	0.025
8	0.028	0.0048	0.122	0.02	0.1686	0.0924
9	0.04	0.005	0.028	0.004	0.034	0.025
10	0.024	0.006	0.026	0.0028	0.046	0.0264
12	0.0158	0.0044	0.028	0.004	0.034	0.016
13	0.006	0.0064	0.024	0.0024	0.0256	0.0172
Total load	0.3346	0.04	0.486	0.0772	0.6932	0.4152

## B. Distribution generation system modeling

Diesel generators, PV system, and WT models were designed for the DG system modeling to show the behavior at normal operations. The detailed system modeling of each DG model to define the reactions of every distributed generator inside the RTDS/RSCAD environment is shown below.

#### 1. Diesel generator model

The diesel generator is a synchronized machine with a governor and an excitation system. The swing equation describes how the rotor moves inside the turbine [41]:

$$\frac{dw}{dt} = \frac{1}{2H} \{ P_m - P_e - \xi(\omega - \omega_o) \} \tag{24}$$

Where  $\omega$  describes the rotor's speed (rad/s), H represents the inertia constant, expressed in seconds.  $P_m$  and  $P_e$  represent the mechanical input power (p.u.) and electrical output power (p.u.), respectively.  $\xi$  indicates the damping force, and  $\omega_o$  represents the rotor's speed (rad/s).

The excitation system generates a variable field voltage  $(E_f)$  of the motor [42], which is described as,

$$\frac{dE_f}{dt} = \frac{1}{\tau_A} \left( V_{ref} - V_t \right) \tag{25}$$

In this equation,  $\tau_A$  means the time constant of the exciter,  $V_{ref}$  is the reference voltage, and  $V_t$  represents the terminal voltage magnitude value. The governor's reaction to the frequency control [43] is provided by

$$\frac{dP_m}{dt} = \frac{1}{\tau_o} \left\{ P_{ref} - P_m - \kappa(\omega - \omega_o) \right\}$$

Here, the Governor time constant is denoted by  $\tau_g$ , and the droop coefficient is represented by  $\kappa$ , while  $P_{ref}$  is referred to as the mechanical power.

### 2. PV system model

A controlled current source for the PV array [44] is set according to the irradiance (G) and the temperature (T). The maximum power  $(P_{maxPV})$  from a solar panel [45] can be found by using the standard PV formula.

$$P_{maxPV} = \eta_{PV} * A_{PV} * G \tag{27}$$

Where  $\eta_{PV}$  and  $A_{PV}$  represent the efficiency and surface area of PV with irradiance ( $\mathcal{G}$ ).

The Maximum Power Point Tracking (MPPT) technique is used to adjust the  $V_{MPPT}$  to obtain the maximum output power from the PV system.

$$\frac{dV_{MPPT}}{dt} = K_p * \frac{dP}{dV} \tag{28}$$

where  $K_p$  is the proportional gain constant. The inverter output is controlled by a UPF; therefore:

$$Q_{PV} = 0, \quad P_{PV} = P_{MPPT} \tag{29}$$

#### 3. Wind turbine generator model

The wind turbine was simulated using the specified aerodynamic power extraction equation [46]:

$$P_{Wind} = \frac{1}{2} \rho A C_p(\lambda, \beta) v_w^3 \tag{30}$$

Where p is the air's density, A refers to the rotor area,  $C_p$  represents the power coefficient, and  $v_w$  means the wind speed (m//s). The tip-speed ratio  $(\lambda)$  is directly proportional to the product of the rotor radius  $(R_r)$  and rotor speed  $(\omega_r)$ , and inversely proportional to the wind speed  $(v_w)$ , which is defined as.

$$\lambda = \frac{R_r * \omega_r}{v_{vv}} \tag{31}$$

A back-to-back converter provides the power to the generator. In a balanced state, the WT delivers active power at a unity power factor.

$$Q_{wind} = 0, P_{wind} = constant$$
 (32)

During overproduction, the plant relies on pitch control to allow the turbines to run at the appropriate speed.

$$\frac{d\beta}{dt} = k_{\beta}(\omega_r - \omega_{rated}) \tag{33}$$

) All these equations together show how each DG

performs in real time and can be built with RTDS/RSCAD's basic components. They give the necessary adjustment ability to ensure proper power supply, voltage, and regular frequency under changing power demands. The power values for the DGs parameter connected to the system are summarized in Table 5.

Table 5: Distribution generation system parameters

System	Maximum capacity	
Main grid	100 MW, 115 kV, 50Hz	
PV Plant	1.74 MW, 13.2 kV	
Wind Generation	0.8 MW, 13.2 kV	
Diesel Generator	3.0 MW, 13.2 kV	

## C. Transformer modification for alternative generation

Transformers rated at 115/4.16 kV and 13.2/4.16 kV are used to regulate voltage levels between distributed generation sources and the connected bus within the distributed generation area. The interconnection of distributed generation with bus nodes is controlled by a switch or a breaker. The installed transformers have a loss of approximately 3% and are connected in a delta-to-star configuration with a neutral reference point of zero (D-YN-0).

#### IV. Result discussion

The proposed Master-Slave DG allocation model is tested on the RTDS with the RSCAD interface. RTDS offers a hardware-in-the-loop (HIL) platform that allows the realistic real-time simulation of microgrid behaviour under various loading conditions. The IEEE 13-bus system is designed using RSCAD, with DG units and control strategies, which are connected to the network through a transformer. Under this arrangement, dynamic responses of the microgrid, including voltage stability and power loss variation, can be dynamically viewed and analyzed. The main purpose of installing a diesel generator is that it should act as a backup to the grid, and its output should be scaled to the requirements of the network. The diesel generator with a capacity of 2.4

kV, 3.125 MVA is linked to a feeder by a 5 MVA stepup transformer that increases the voltage from 2.4 kV to 4.16 kV. The microgrid operates at 4.16 kV with a frequency of 50 Hz. The RTDS/RSCAD platform was used to simulate grid-connected conditions at different load conditions. The outcomes validate the conclusions that the proposed optimization, as it is implemented in cooperation with the Master-Slave control strategy, works efficiently to improve the performance of a microgrid. The RTDS/RSCAD is used so that the approach is not limited to theoretical simulation but is also practical and applicable to realworld operations of microgrids. The integration of distributed generation systems helps reduce power losses, but it can also negatively impact the voltage levels. An effective interconnection of DG units is necessary to ensure maximum performance and a better voltage profile. As shown in Fig. 2, the optimal locations for integrating distributed generation are bus 3 for the diesel generator, bus 6 for wind energy, and bus 8 for the PV array.

## A. Variation in active and reactive power profile

Active power fluctuations under load conditions 1, 2, and 3 are individually shown in Figs. 3, 4, and 5. The system updates lead to significant adjustments to the active power levels. In load scenario 1, solar and wind systems are operating and providing all the required energy, while the diesel generator and grid are not in use, as seen in fig. 3. In load scenario 2, where demand becomes higher, all the maximum power is provided by the PV system, and the remaining power is given by the diesel generator, wind, and utility grid, as shown in Fig. 4. Likewise, during load scenario 3 when demand rises, each source is contributed the supply. Most of the energy is supplied by the diesel generator, followed by the PV source, while a small amount of power is supplied by the wind and grid, as depicted in Fig. 5. These corresponding variations in the reactive profiles are depicted in Figs. 3, 4, and 5. Although the efficiency of the system has improved, there is no appreciable effect on reactive power. The cause is the absence of reactive power from the DG on the grid.

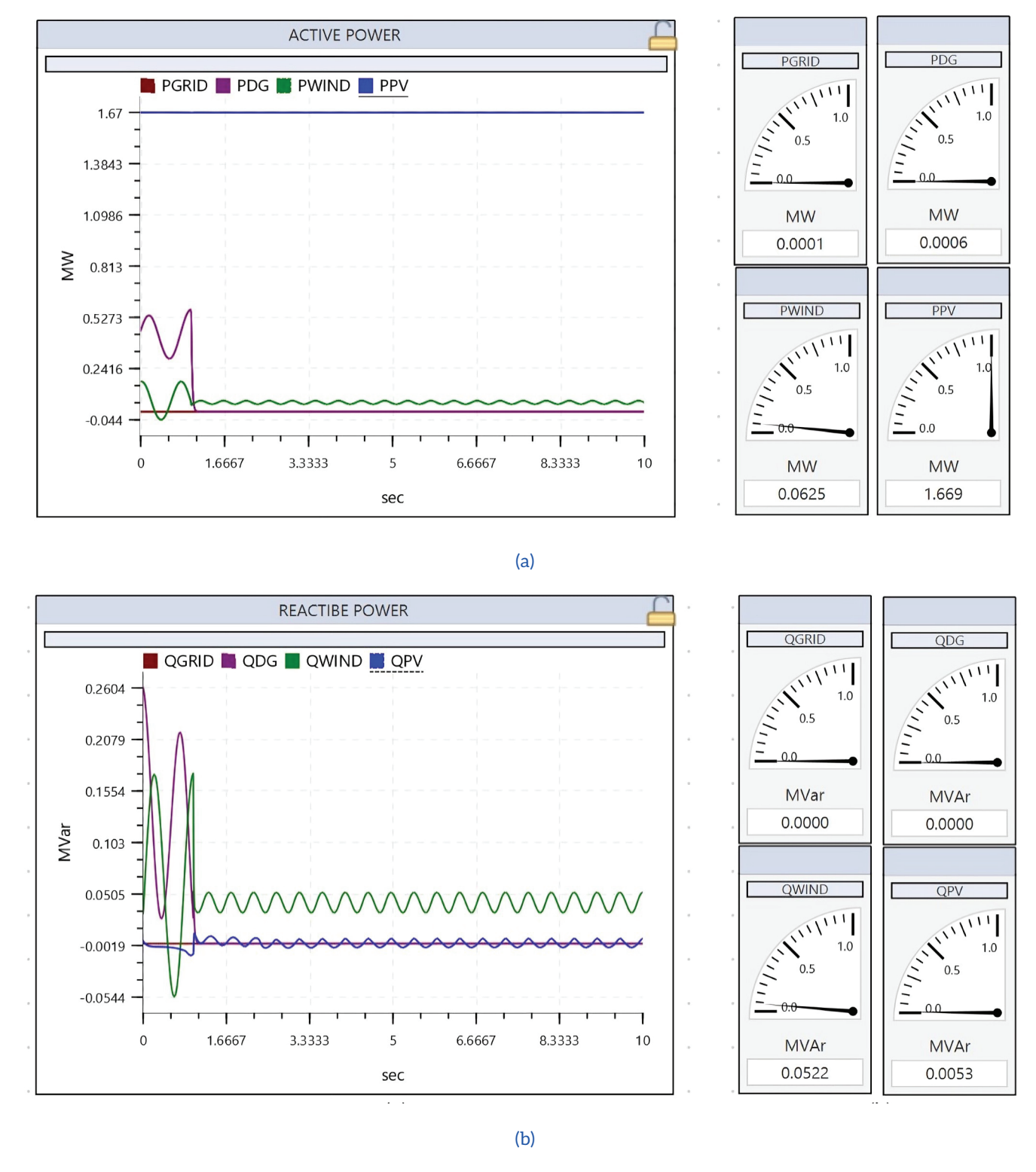
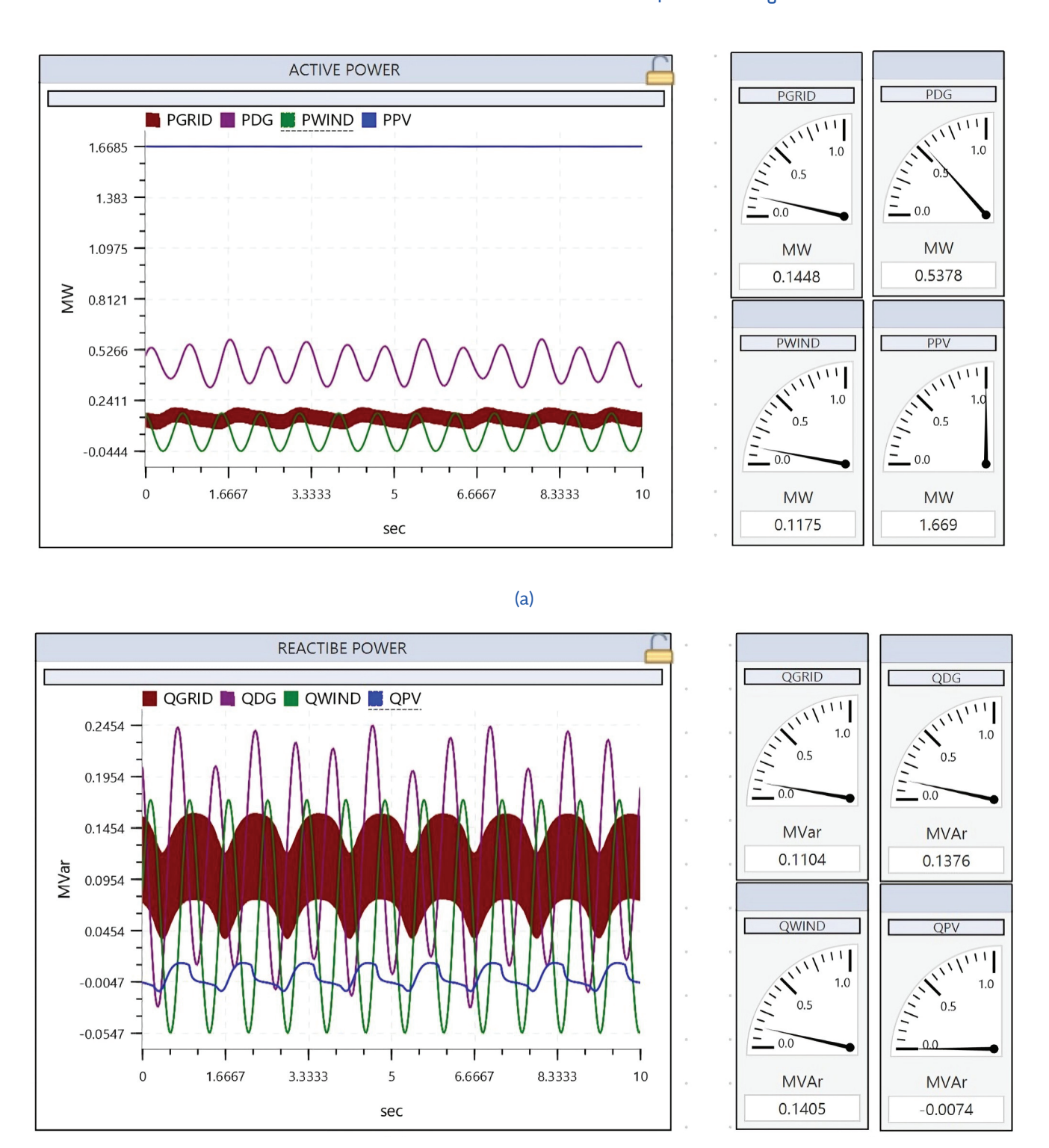


Figure 3: Variation in generation for load scenario 1 (a) active power profile (b) reactive power profile.



(b) Figure 4: Variation in generation for load scenario 2 (a) active power profile (b) reactive power profile.

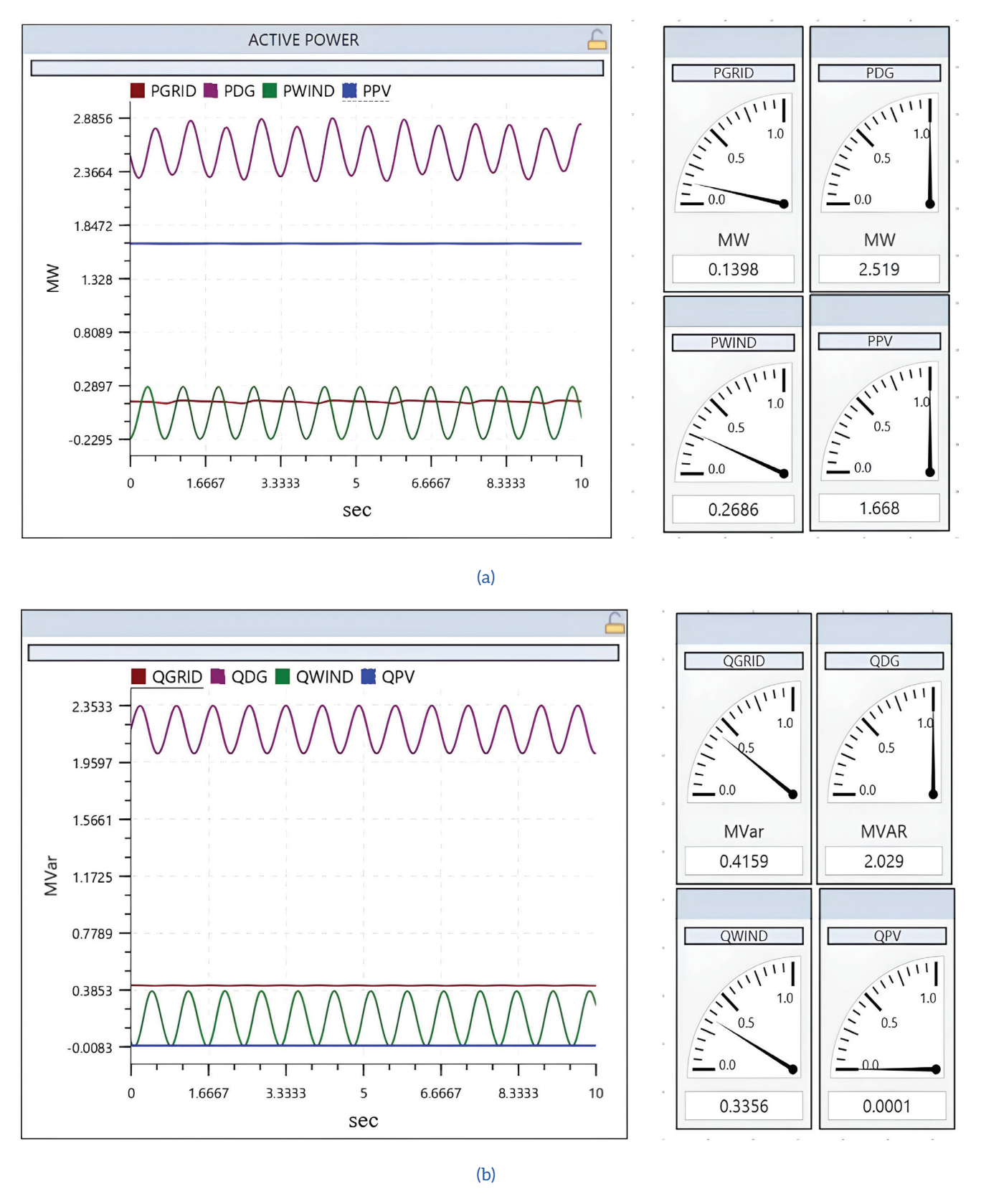


Figure 5: Variation in generation for load scenario 3 (a) active power profile (b) reactive power profile.

#### B. Variation in power losses

#### Case study 1:

This case study focuses on the results of the use

of a WT as a distributed generator in the system. The PSO-FDLF optimization is used to find out the position and size of the DG units, which helps to enhance the voltage and reduce the overall power

losses. Real and reactive power losses are illustrated in Fig. 6 (a) and Fig. 7(b) for the IEEE 13-bus system in three conditions: without DG, with DG controlled by PSO-NR, and with DG controlled by PSO-FDLF.

The lack of DG causes greater power losses, with buses 3, 6, and 8 experiencing the largest increases, compared to all other buses.

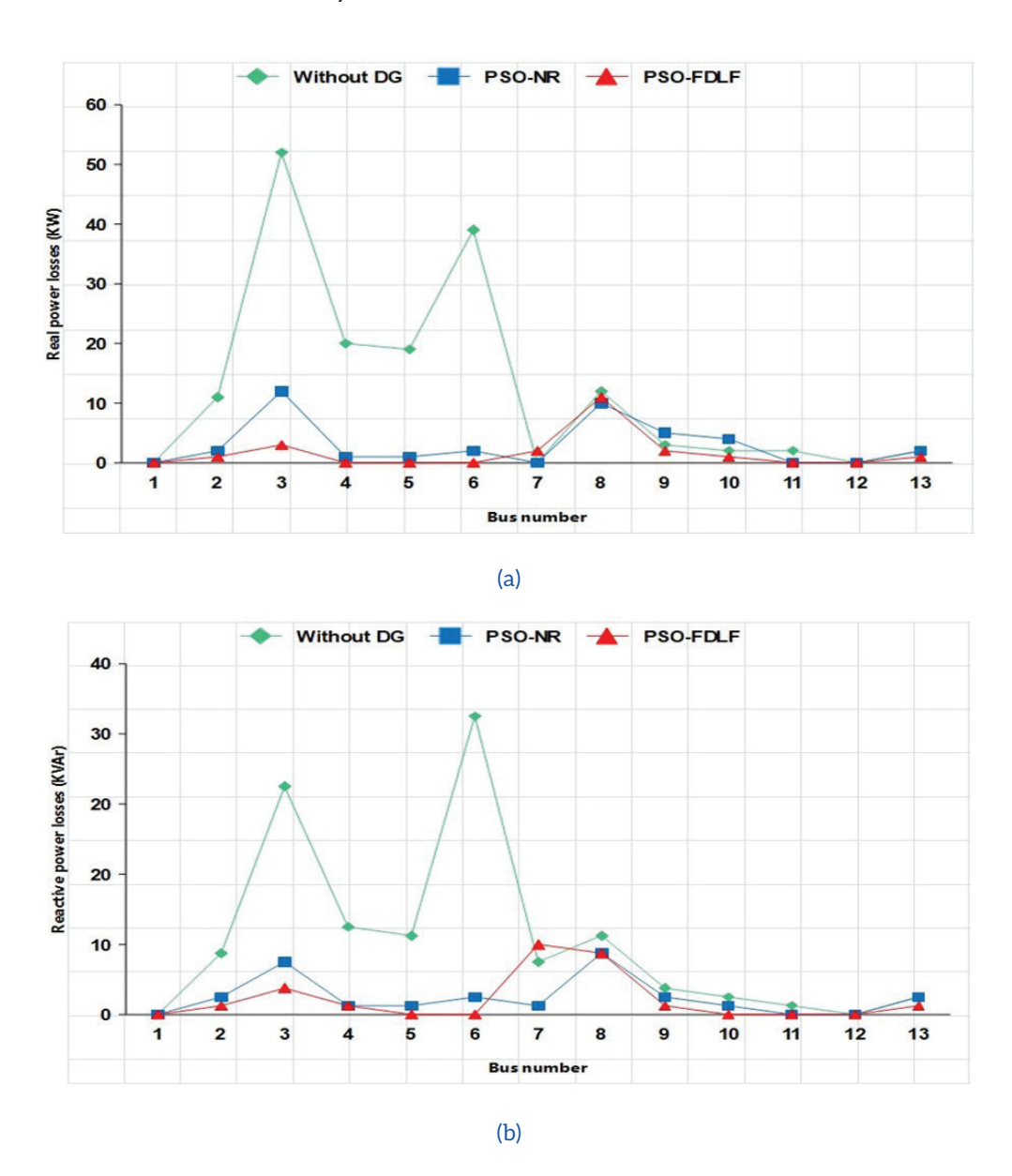


Figure 6: (a) Real power losses (b) Reactive power losses for the 13-bus using PV.

The active and reactive power losses are substantially decreased because of the use of PSO-NR and PSO-FDLF optimization techniques. Among the two methods, PSO-FDLF has less loss, which means that it is able to save energy and increase efficiency.

#### Case study 2:

In the WT configuration, the active and reactive power losses in the IEEE 13 bus system occur as shown in Fig. 7(a) and Fig. 7(b). The study concentrated on finding the correct placement and

size of WTs to cut down on energy waste within the network. The grid that does not contain the DG has higher losses throughout the entire system, especially at buses 3, 6, and 8.

When using the PSO-NR and PSO-FDLF algorithms, both active and reactive losses are reduced, but PSO-FDLF gives the greatest loss reduction. As a result, the optimization of WT integration leads to a better performance of the entire distribution system.

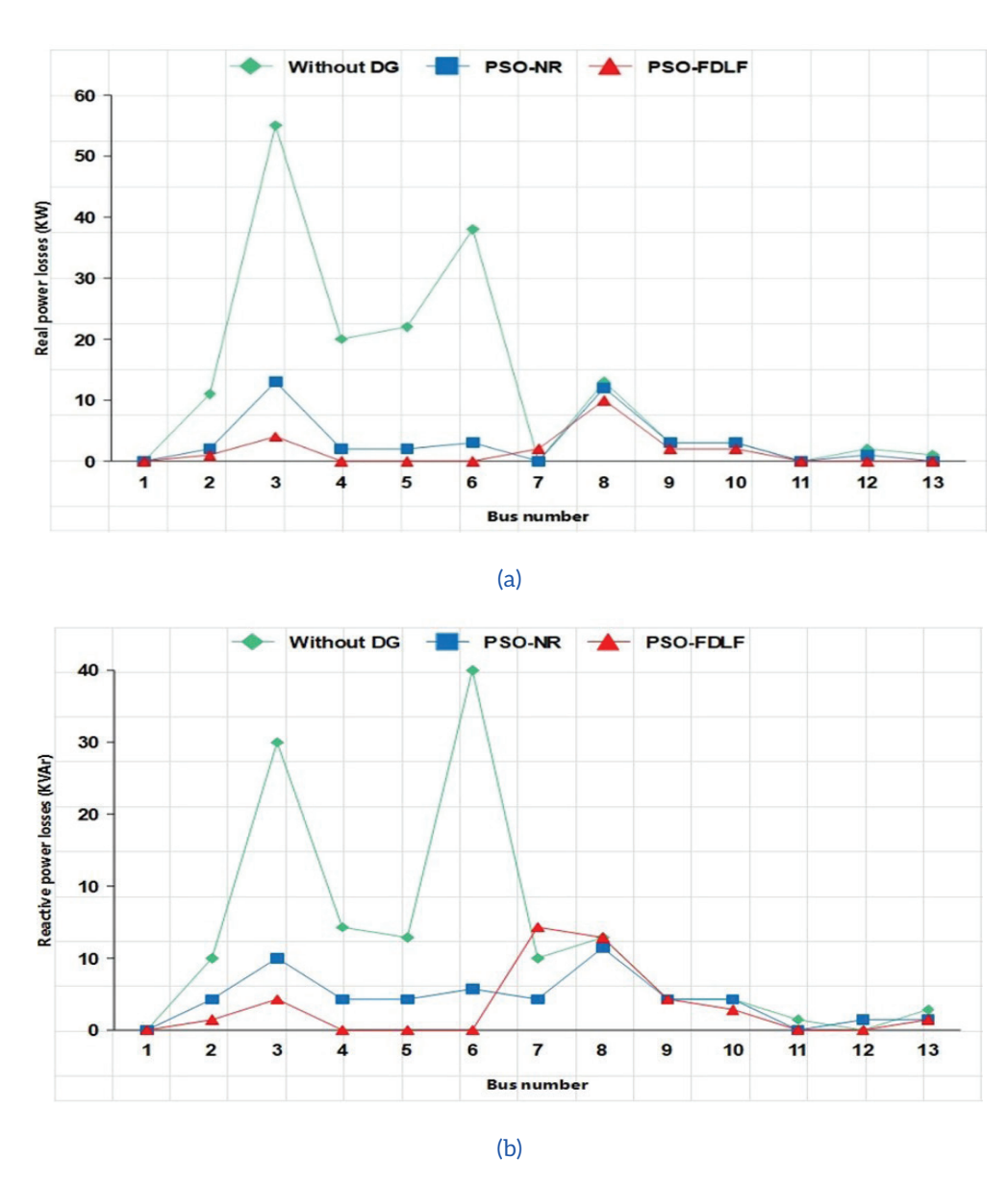


Figure 7: (a) Real power losses (b) Reactive power losses for the 13-bus using WT.

#### Case study 3:

PV and WT were used as DGs and tested on an IEEE-13 bus in this case to attain an efficient integration of the RES. The integration of DG units, specifically, PV and WT, resulted in a significant enhancement of the overall network voltage profiles. As shown in Fig. 8 (a) and (b), the graphical data represent the significant reduction in real and reactive power losses across

the network following the incorporation of PV and WT DGs. The active and reactive power losses are illustrated in Tables 6 and 7, respectively. The total power losses are decreased through the collective optimization, without the involvement of DG. The reactive power losses followed a similar pattern, dropping dramatically from the initial level.

Table 7: Reactive Power Losses (kVAr)

Table 6: Active Power Losses (kW)

Without DG PSO-NR PSO-FDLF **PSO-NR PSO-FDLF** Without DG 

bus Nulliber	Without DG	P2O-IVK	P3O-FDI
1	0	0	0
2	6	3	2
3	30	10	4
4	13	4	1
5	11	2	1
6	32	3	2
7	10	5	9
8	9	6	8
9	5	3	3
10	3	1	1
11	1	0	0
12	1	1	1
13	2	3	2

**Bus Number** 1,7&11 

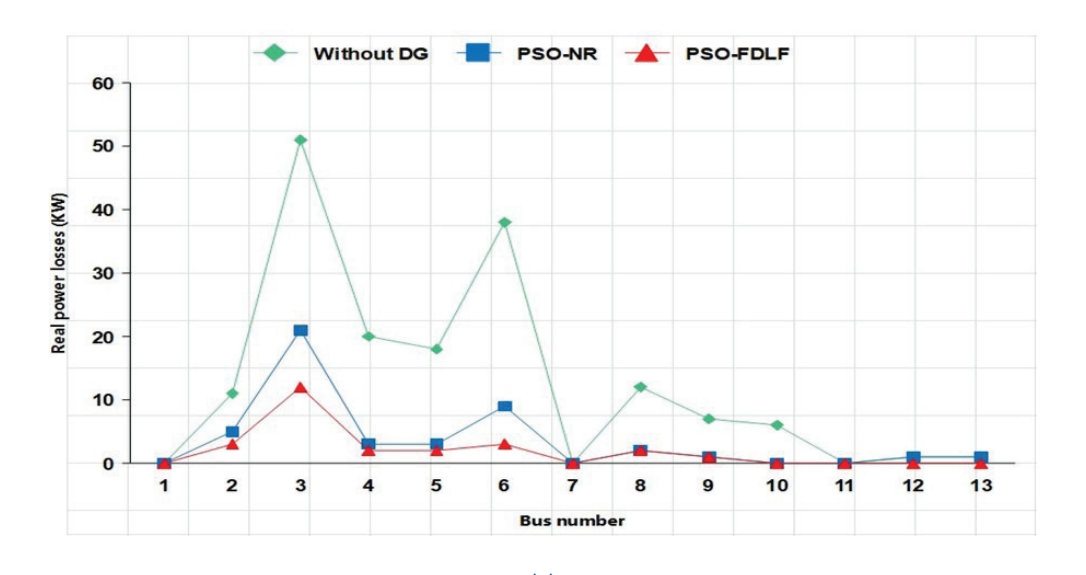




Figure 8: (a) Real power losses (b) Reactive power losses for the 13-bus system using PV and WT.

(b)

Significantly, the PSO-FDLF algorithm demonstrates the greatest reduction in loss, showing its effectiveness in addressing the multi-source DG optimization problem using the MS method. In addition to the reduction of real and reactive power losses, the results also show that the PSO-FDLF framework increases the weakest bus voltage, especially under heavy loading conditions. The proposed PSO-FDLF algorithm obtained voltage stability margins that are 3-5% better than PSO-NR and power losses up to 40% lower for critical buses. These enhancements are ascribed to the complementarity between swarm-based exploration and the fast convergence of FDLF, which makes the approach computationally efficient and operationally viable. Importantly, the RTDS/RSCAD real-time implementation confirms that the optimization is not just applicable to the offline simulations but can be used as well in the actual microgrid operation.

#### C. Variation in voltage profile

The voltage profiles of the 13-bus distribution network under three different loading conditions are shown in Figs. 9, 10, and 11. The effect of incorporating DG, specifically via optimization techniques such as PSO-NR and PSO-FDLF, is examined in comparison to the baseline situation without DG. The master DG at bus three is selected in the master mode, and the slave DG installed at buses 6 and 8 is selected in the slave mode. In the conditions of the load scenario 1, the voltage level is maximal at buses 3, 6, and 8, and minimal at bus 13. Voltage reductions are clearly minimized with the incorporation of optimized DGs through PSO-NR and PSO-FDLF. The minimum voltages, without DG, are observed to be: 0.90 p.u. The PSO-NR records 0.96 p.u. The PSO-FDLF is characterized by a value of 0.970 p.u. as illustrated in Fig. 9.



Figure 9: Variation in voltage profile for load scenario 1 using PV as a DG.

In load condition 2, voltage is relatively high at buses 3, 6, and 8, and the minimum levels are again at bus 13, as shown in Fig. 10. The DG interconnection increases the minimum voltage levels to 0.90 p.u. Without DG, 0.965 p.u. with PSO-NR, and 0.975 p.u.

with PSO-FDLF. The voltage profiles enhancement depicts that the PSO-FDLF algorithm works steadily regardless of the load level to ensure that the voltage level does not drop below the acceptable level.

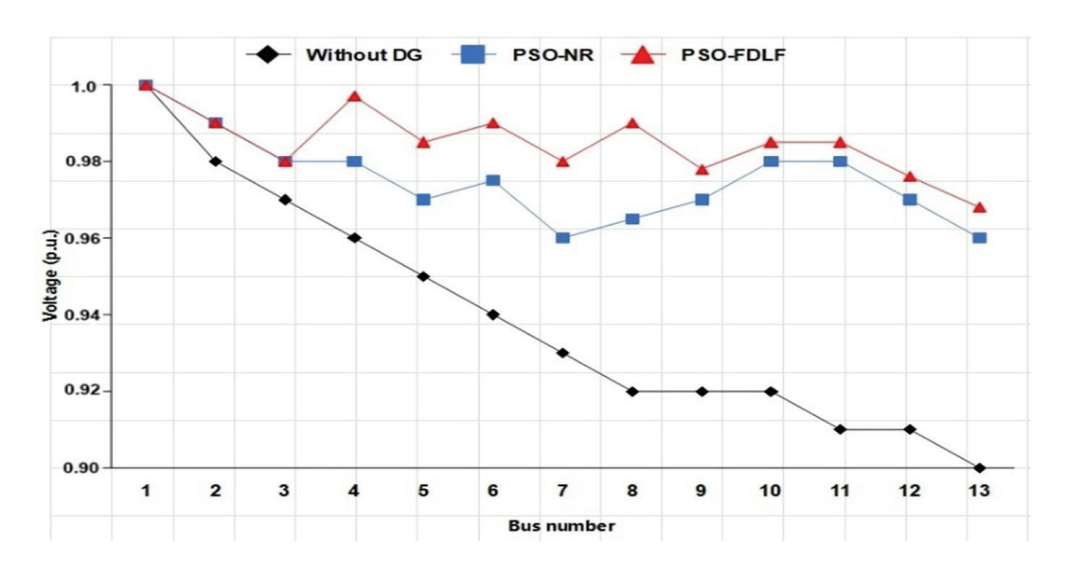


Figure 10: Variation in voltage profile for load scenario 2 using WT as a DG.

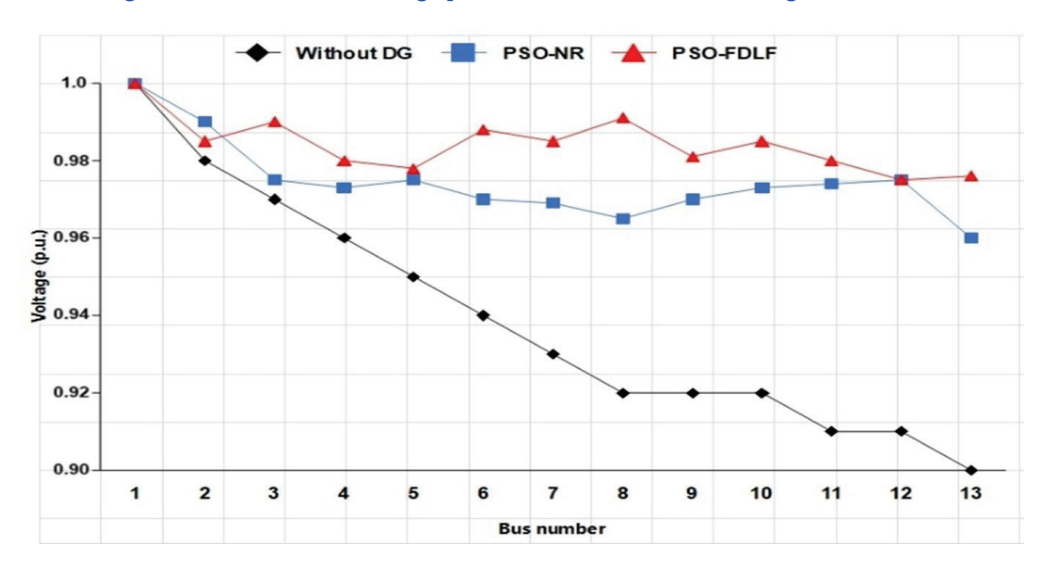


Figure 11: Variation in voltage profile for load scenario 2 using PV & WT as DG.

Under a load condition 3, buses 3, 6, and 8 continue to show the peak voltage values, and bus 13 again shows the lowest voltage. The voltage of the DG-assisted system is summarized as follows: no DG at 0.90 p.u., PSO-NR at 0.965 p.u., and PSO-FDLF at 0.973 p.u., as depicted in Fig. 11. The obtained results show that hybrid-optimized FDLF has the ability to maintain the voltage stability of a pressurized power system. The results demonstrate that PSO-FDLF offers better voltage support than PSO-NR and the conventional alternative. The inclusion of a DG in the power system maintains the voltage level near the standard value of 1.0 p.u., thereby enhancing voltage stability and system dependability.

The obtained results evidently show that the proposed MS algorithm with the PSO-FDLF algorithm is superior to the conventional PSO-NR

method in terms of reducing the power losses and enhancing the voltage stability in the IEEE 13-bus test system. The PSO-FDLF produced lower active and reactive power losses than the other types under different loading scenarios, as illustrated in Tables 6 and 7; furthermore, the PSO-FDLF produced a voltage profile closer to the nominal value of 1.0 p.u., as depicted in Figs. 9-11. The advantages of this optimization technique are validated by improving efficiency with respect to the operational mode of DGs (Master and Slave) as well as by the optimized placement when compared to methods that assume all DGs working at unity power factor.

### V. Conclusion

This research developed and validated a Master-Slave approach for distributed generation allocation strategy combined with the PSO-FDLF optimization method for microgrid operation. Unlike traditional DG allocation techniques, the MS framework allows one DG to work at a non-unity power factor (Master), and other DGs can be operated at unity power factor (Slaves). This configuration, which was tested on the system with the IEEE-13 bus system, showed significant performance improvements. The results show that the proposed approach reduces the real power losses by up to 77% with respect to the base case without DGs and 45% with respect to PSO-NR optimization. Furthermore, the minimum bus voltage improved from 0.90 p.u. to 0.973 p.u., which kept the values within acceptable limits under all loading conditions. The proposed method also produced voltage stability margins as much as 3% to 5% higher than conventional allocation methods.

Results from real-time implementation on RTDS/RSCAD proved the potential of the proposed method, with stable operation observed, keeping the voltage fluctuations within ± 3% of nominal values under variable load conditions. These findings validate the proposed optimization framework based on MS to improve the efficiency, stability, and reliability of the operation of microgrids as a scalable solution for power distribution systems integrated with renewable energy sources in the future.

#### References

- [1] A. Muntaser, H. Ragb, and I. Elwrfalli, "DC Microgrid Based on Battery, Photovoltaic, and Fuel Cells; Design and Control," Dec. 28, 2022. doi: 10.20944/preprints202212.0527.v1.
- [2] K. Nagaraju, S. Sivanagaraju, T. Ramana, and V. Ganesh, "Enhancement of Voltage Stability in Distribution Systems by Optimal Placement of Distribution Generator," Distributed Generation & Alternative Energy Journal, vol. 27, no. 2, pp. 25–41, Apr. 2012, doi: 10.1080/21563306.2012.10505410.
- [3] L. F. Grisales, A. Grajales, O. D. Montoya, R. A. Hincapie, and M. Granada, "Optimal location and sizing of Distributed Generators using a hybrid methodology and considering different technologies," in 2015 IEEE 6th Latin American Symposium on Circuits & Systems (LASCAS), IEEE, Feb. 2015, pp. 1–4. doi: 10.1109/LASCAS.2015.7250486.

#### Future Scope:

Future research will include economic considerations, such as investment and operational costs, in the proposed MS-PSOP-FDLF framework for a complete cost-benefit analysis. The proposed framework will be compared with other sophisticated optimization techniques such as the WOA, GA, DEO, and SMA methods. Algorithms will be evaluated to see if hybrid algorithms that combine the benefits from multiple algorithms can improve DG allocation performance. This will provide a more complete evaluation of the technical and economic benefits of the practical microgrid planning.

#### Acknowledgments:

The author would like to heartily acknowledge Dr. Ikbal Ali and Dr. Anwar Shahzad Siddiqui, whose guidance, encouragement, and support in this research work are invaluable. Their valuable recommendations and continued encouragement were helpful in developing the study, especially on the exploration and implementation of the RTDS platform.

#### Authors' contribution:

**Sunil Kumar:** Writing-original draft, visualization, methodology, formal analysis, data curation, and conceptualization. **Ikbal Ali**: Supervision. **Anwar Shahzad Siddiqui**: Supervision.

- [4] S. M. Abu, M. A. Hannan, M. Mansor, P. J. Ker, and C. Yaw Long, "Optimized Intelligent Controller for Energy Storage based Microgrid towards Sustainable Energy Future," in 2023 IEEE International Conference on Energy Technologies for Future Grids (ETFG), IEEE, Dec. 2023, pp. 1–7. doi: 10.1109/ETFG55873.2023.10407475.
- [5] S. Kumar, S. Sharma, I. Ali, and A. S. Siddiqui, "Real-Time Performance Assessment of Electric Vehicle Charging Stations with RTDS," in 2025 IEEE International Students' Conference on Electrical, Electronics and Computer Science (SCEECS), IEEE, Jan. 2025, pp. 1–6. doi: 10.1109/ SCEECS64059.2025.10940406.
- [6] Y. Wang, H. Ji, R. Luo, B. Liu, and Y. Wu, "Energy Optimization Strategy for Wind-Solar-Storage Systems with a Storage Battery Configuration," *Mathematics*, vol. 13, no. 11, p. 1755, May 2025, doi: 10.3390/math13111755.

- [7] J. J. Kim and J. H. Park, "A Novel Structure of a Power System Stabilizer for Microgrids," *Energies (Basel)*, vol. 14, no. 4, p. 905, Feb. 2021, doi: 10.3390/en14040905.
- [8] X. Lu, J. Wang, and L. Guo, "Using microgrids to enhance energy security and resilience," *The Electricity Journal*, vol. 29, no. 10, pp. 8–15, Dec. 2016, doi: 10.1016/j.tej.2016.11.013.
- [9] A. Firdaus and M. Molinas, "Design and Expansion Planning of Parallel Inverter Based AC Microgrids - An Approach for Improved Stability Margins," Sep. 02, 2020. doi: 10.36227/ techrxiv.12894926.v1.
- [10] M. Mahdavi, A. Awaafo, K. Schmitt, M. Chamana, F. Jurado, and S. Bayne, "An Effective Formulation for Minimizing Distribution Network Costs Through Distributed Generation Allocation in Systems With Variable Loads," *IEEE Trans Ind Appl*, vol. 60, no. 4, pp. 5671–5680, Jul. 2024, doi: 10.1109/TIA.2024.3382255.
- [11] I. P. Nikolakakos, H. H. Zeineldin, M. S. El-Moursi, and N. D. Hatziargyriou, "Stability Evaluation of Interconnected Multi-Inverter Microgrids Through Critical Clusters," *IEEE Transactions on Power Systems*, vol. 31, no. 4, pp. 3060–3072, Jul. 2016, doi: 10.1109/TPWRS.2015.2476826.
- [12] X. Tang, W. Deng, and Z. Qi, "Investigation of the Dynamic Stability of Microgrid," *IEEE Transactions on Power Systems*, vol. 29, no. 2, pp. 698–706, Mar. 2014, doi: 10.1109/TPWRS.2013.2285585.
- [13] J. He, Y. W. Li, R. Wang, and C. Zhang, "Analysis and Mitigation of Resonance Propagation in Grid-Connected and Islanding Microgrids," *IEEE Transactions on Energy Conversion*, vol. 30, no. 1, pp. 70–81, Mar. 2015, doi: 10.1109/TEC.2014.2332497.
- [14] A. Micallef, M. Apap, C. Spiteri-Staines, and J. M. Guerrero, "Mitigation of Harmonics in Grid-Connected and Islanded Microgrids Via Virtual Admittances and Impedances," *IEEE Trans Smart Grid*, pp. 1–11, 2015, doi: 10.1109/TSG.2015.2497409.

- [15] A. Khodaei, S. Bahramirad, and M. Shahidehpour, "Microgrid Planning Under Uncertainty," *IEEE Transactions on Power Systems*, vol. 30, no. 5, pp. 2417–2425, Sep. 2015, doi: 10.1109/TPWRS.2014.2361094.
- [16] S. Ganguly and D. Samajpati, "Distributed Generation Allocation on Radial Distribution Networks Under Uncertainties of Load and Generation Using Genetic Algorithm," *IEEE Trans Sustain Energy*, vol. 6, no. 3, pp. 688–697, Jul. 2015, doi: 10.1109/TSTE.2015.2406915.
- [17] X. Zong and Y. Yuan, "Two-stage robust optimization of regional integrated energy systems considering uncertainties of distributed energy stations," Front Energy Res, vol. 11, Mar. 2023, doi: 10.3389/fenrg.2023.1135056.
- [18] E. I. El-sayed, M. M. Al-Gazzar, M. S. Seif, and A. M. A. Soliman, "Energy management of renewable energy sources incorporating with energy storage device," *International Journal of Power Electronics and Drive Systems (IJPEDS)*, vol. 13, no. 2, p. 883, Jun. 2022, doi: 10.11591/ijpeds.v13.i2.pp883-899.
- [19] A. S. Chaitra and H. R. Sudarshana Reddy, "Improving Reliability in Distribution Systems through Optimal Allocation of Distributed Generators, Network Reconfiguration and Capacitor Placement," SN Comput Sci, vol. 5, no. 5, p. 456, Apr. 2024, doi: 10.1007/s42979-024-02753-0.
- [20] S. Ahmad and A. ul Asar, "Reliability Enhancement of Electric Distribution Network Using Optimal Placement of Distributed Generation," *Sustainability*, vol. 13, no. 20, p. 11407, Oct. 2021, doi: 10.3390/su132011407.
- [21] D. Yu, J. Hao, J. Wang, J. Zhu, Y. Gao, and M. Shaker, "Optimal planning of Microgrids using portfolio optimization with considering uncertainty," *Sustainable Energy Technologies and Assessments*, vol. 58, p. 103323, Aug. 2023, doi: 10.1016/j.seta.2023.103323.
- [22] P.Singh, N.K.Singh, and A.K.Singh, "Intelligent hybrid method to predict generated power of solar PV system," *Renewable Energy and Sustainable Development*, vol. 11, no. 1, p. 141, May 2025, doi: 10.21622/resd.2025.11.1.1264.

- [23] R. T. Moyo, M. Dewa, H. F. M. Romero, V. A. Gómez, J. I. M. Aragonés, and L. Hernández-Callejo, "An adaptive neuro-fuzzy inference scheme for defect detection and classification of solar PV cells," Renewable Energy and Sustainable Development, vol. 10, no. 2, p. 218, Sep. 2024, doi: 10.21622/resd.2024.10.2.929.
- [24] R. T. Moyo and M. Dewa, "The role of computational intelligence techniques in the advancements of solar photovoltaic systems for sustainable development: a review," Renewable Energy and Sustainable Development, vol. 8, no. 2, p. 52, Dec. 2022, doi: 10.21622/resd.2022.08.2.052.
- [25] S. A. Arefifar and Y. A.-R. I. Mohamed, "DG Mix, Reactive Sources and Energy Storage Units for Optimizing Microgrid Reliability and Supply Security," IEEE Trans Smart Grid, vol. 5, no. 4, pp. 1835–1844, Jul. 2014, doi: 10.1109/ TSG.2014.2307919.
- [26] M. Abbasi, M. Hedayatpour, and A. G. Garganeev, "Microgrid Voltage and Frequency Control Using Droop Control Based on Master/ Slave Method," in 2020 21st International Conference of Young Specialists on Micro/ Nanotechnologies and Electron Devices (EDM), IEEE, Jun. 2020, pp. 367-373. doi: 10.1109/ EDM49804.2020.9153493.
- [27] A. M. Pasha, H. H. Zeineldin, E. F. El-Saadany, and S. S. Alkaabi, "Optimal allocation of distributed generation for planning masterslave controlled microgrids," IET Generation, Transmission & Distribution, vol. 13, no. 16, pp. 3704-3712, Aug. 2019, doi: 10.1049/ietgtd.2018.5872.
- [28] S. Oviedo-Carranza, J. S. Artal-Sevil, and J. A. Domínguez-Navarro, "Optimal Operation of a Distributed Generation Microgrid based on the Multi-Objective Genetic Algorithms," Renewable Energy and Power Quality Journal, vol. 20, pp. 789-794, Sep. 2022, doi: 10.24084/ repqj20.436.
- [29] S. M. R. H. Shawon, X. Liang, and M. Janbakhsh, "Optimal Placement of Distributed Generation Units for Microgrid Planning in Distribution Networks," IEEE Trans Ind Appl, vol. 59, no. 3, pp. 2785-2795, May 2023, doi: 10.1109/ TIA.2023.3236363.

- [30] S. He and J. Liu, "Optimal Allocation Stochastic Model of Distributed Generation Considering Demand Response," Energies (Basel), vol. 17, no. 4, p. 795, Feb. 2024, doi: 10.3390/en17040795.
- P. Kant, P. Singhal, S. Kumar, and S. Gupta, "DC [31] microgrid designed for the integration of wind and solar energy sources," 2023, p. 020077. doi: 10.1063/5.0122979.
- [32] Y. Khalid Hamad, A. Nasser Hussain, Y. N. Lafta, A. Al-Naji, and J. Chahl, "Multi-Objective Optimization of Renewable Distributed Generation Placement Sizing for Technical and Economic Benefits Improvement in Distribution System," IEEE Access, vol. 12, pp. 164226-164247, 2024, doi: 10.1109/ACCESS.2024.3492119.
- [33] S. Kumar, R. Agarwal, and H. Subhadra, "Adaptive bayesian sparse polynomial chaos expansion for voltage balance of an isolated microgrid at peak load," Renewable Energy and Sustainable Development, vol. 11, no. 1, p. 161, Jun. 2025, doi: 10.21622/resd.2025.11.1.1281.
- [34] S. Kumar, I. Ali, and A. S. Siddiqui, "Energy management in a grid-connected microgrid using hybrid Golden Jackal optimization and gradient descent optimization and the concept of loadability," e-Prime - Advances in Electrical Engineering, Electronics and Energy, vol. 9, p. 100763, Sep. 2024, doi: 10.1016/j. prime.2024.100763.
- M. Miller, J. L. Paternina, S. F. Contreras, C. A. [35] Cortes, and J. M. A. Myrzik, "Optimal allocation of renewable energy systems in a weak distribution network," Electric Power Systems Research, vol. 235, p. 110649, Oct. 2024, doi: 10.1016/j.epsr.2024.110649.
- [36] F. Agha Kassab, R. Rodriguez, B. Celik, F. Locment, and M. Sechilariu, "A Comprehensive Review of Sizing and Energy Management Strategies for Optimal Planning of Microgrids with PV and Other Renewable Integration," Applied Sciences, vol. 14, no. 22, p. 10479, Nov. 2024, doi: 10.3390/app142210479.
- M. Rahimian, L. D. Iulo, and J. M. P. Duarte, [37] "A Review of Predictive Software for the Design of Community Microgrids," Journal of Engineering, vol. 2018, pp. 1-13, 2018, doi: http://apc.aast.edu 10.1155/2018/5350981.

- [38] N. Ghanbari, H. Mokhtari, and S. Bhattacharya, "Optimizing Operation Indices Considering Different Types of Distributed Generation in Microgrid Applications," *Energies (Basel)*, vol. 11, no. 4, p. 894, Apr. 2018, doi: 10.3390/en11040894.
- [39] O. A. Afolabi, W. H. Ali, P. Cofie, J. Fuller, P. Obiomon, and E. S. Kolawole, "Analysis of the Load Flow Problem in Power System Planning Studies," *Energy Power Eng*, vol. 07, no. 10, pp. 509–523, 2015, doi: 10.4236/epe.2015.710048.
- [40] L. Kumar, M. Pandey, and M. K. Ahirwal, "Parallel Global Best-Worst Particle Swarm Optimization Algorithm for solving optimization problems," *Appl Soft Comput*, vol. 142, p. 110329, Jul. 2023, doi: 10.1016/j. asoc.2023.110329.
- [41] C. Shah, R. W. Wies, T. M. Hansen, R. Tonkoski, M. Shirazi, and P. Cicilio, "High-Fidelity Model of Stand-Alone Diesel Electric Generator With Hybrid Turbine-Governor Configuration for Microgrid Studies," *IEEE Access*, vol. 10, pp. 110537–110547, 2022, doi: 10.1109/ ACCESS.2022.3211300.
- [42] A. M. Haval and M. Afzal, "Power System Stability Improvement Through PV Integration and Unified Power Flow Control," *E3S Web of Conferences*, vol. 564, p. 05018, Sep. 2024, doi: 10.1051/e3sconf/202456405018.

- [43] X. Chen, H. Dong, and Y. Zhang, "A New Power System Frequency Response Model with Different Types of Generator Units," in 2022 3rd International Conference on Advanced Electrical and Energy Systems (AEES), IEEE, Sep. 2022, pp. 121–127. doi: 10.1109/AEES56284.2022.10079681.
- [44] S. Kumar, I. Ali, and A. S. Siddiqui, "Performance Analysis of Different Solar Models Based on the Solar cell Parameters," *Indian Journal of Pure & Applied Physics*, 2021, doi: 10.56042/ijpap.v59i3.67765.
- [45] G. N. Gusev, O. V. Zhdaneev, M. E. Gainullin, A. Y. Argastsev, and D. N. Lapkin, "Solar PV system with maximum power tracking," *Int J Hydrogen Energy*, vol. 87, pp. 258–267, Oct. 2024, doi: 10.1016/j.ijhydene.2024.08.441.
- [46] S. Kumar, I. Ali, and A. S. Siddiqui, "Real Time Performance Assessment of Wind Turbine Model Under Ferro Resonance Conditions," in 2024 IEEE 16th International Conference on Computational Intelligence and Communication Networks (CICN), IEEE, Dec. 2024, pp. 755–760. doi: 10.1109/CICN63059.2024.10847454.